JOURNAL OF MATERIALS SCIENCE 32 (1997) 3451–3456

Grain boundary sliding contribution to superplastic deformation in alumina–zirconia composites

O. FLACHER, J. J. BLANDIN
Génie Physique et Mécanique des Matériaux, I.N.P.G./U.J.F., E.N.S. de Physique de Grenoble, ESA CNRS 5010, BP 46 - 38402 Saint-Martin d'Hères Cedex, France

Superplastic deformation in compression has been performed on Al_2O_3–ZrO_2 laminated composites with volume fractions of zirconia from 0 to 20%. In the as-sintered condition, the materials exhibit a fine-grained (0.2 μm) microstructure, but show differences in residual porosity depending on the zirconia content. The grain boundary sliding (GBS) contribution is known to be the main mechanism of deformation in the superplastic regime. Its contribution to the total deformation can be obtained from the knowledge of the intragranular deformation and from the strain due to densification. The contribution of the intragranular deformation was estimated by two different methods, namely the measurement of the grain shape variation and the change in the crystallographic texture of alumina. The reliability of the two methods are discussed since some differences are observed. The higher GBS contribution in the materials which exhibit the lower residual porosity is also discussed.

1. Introduction

One of the most important problems in developing ceramic materials is related to their formability into useful components. For this forming, superplasticity permits substantial shape flexibility and good dimensional accuracy. There is general agreement that grain boundary sliding (GBS) is one of the major strain contributing mechanisms of flow in superplastic deformation [1–6] since its contribution to the total strain usually exceeds 50% in ceramic materials [7, 8]. Besides, it has been shown [7, 9] that the sliding contribution to creep increases with decreasing grain size of the material.

During superplastic deformation, conventional plasticity also takes place (diffusion, intragranular dislocation slip (IDS)) but its contribution to the total strain remains limited. Experimental evidence for the development of IDS during superplastic deformation of alumina were obtained via transmission electron microscopy (TEM) [10]. Data concerning the GBS contribution can be deduced from measurements of the offsets in marker lines, or indirectly by the estimation of the IDS contribution from various techniques, like the change in grain shape [7] or the variation in crystallographic texture [3, 6]. A basal texture has already been reported during the superplastic flow of alumina, since the basal slip ($(0\,0\,1)\langle 1\,1\,0\rangle$) has the lowest critical resolved shear stress [6] at the conventional temperatures of superplastic deformation.

The aim of this paper is to estimate the GBS contribution to the total deformation during superplastic creep of ultrafine grained alumina–zirconia composites with particular attention to the influence of the residual porosity.

2. Materials and experimental procedures

Al_2O_3–ZrO_2 composites containing 0 (AZ0), 5 (AZ5), 10 (AZ10) and 20 (AZ20) vol % of zirconia have been investigated. Pure alumina (Sumitomo AKP-50) and zirconia without any dopant (Tosoh TZ-0) were used as starting powders. Composites were prepared by a tape casting route, consisting of stacking approximately 50 tapes, followed by thermocompression and uniaxial sintering (20 MPa, 100 min, 1300 °C). Densities of the sintered bodies were measured by the Archimedes' method.

The microstructures were characterized by transmission electron microscopy (TEM, Jeol 200 CX) of thin foils taken perpendicular to the plane of the tapes, but the loading direction was not marked. The foils were prepared by standard ion milling procedures, followed by carbon coating. Mean grain sizes, $\langle d\rangle$, were measured by image analysis (Image Proplus software) performed on TEM micrographs, according to $\langle d\rangle = 1.38(\langle S\rangle)^{1/2}$, with $\langle S\rangle$ the average grain section area. The intercept lengths of the grains (L) were measured along various directions in order to determine the maximum (L_{max}) and the minimum (L_{min}) values. In the initial state and in the deformed state, a shape parameter (Sh) was thus determined as the ratio L_{max}/L_{min}.

Tests were performed at constant strain rate in air by uniaxial compression at 1300, 1350 and 1400 °C. Initial dimensions of the samples were approximately $3.5 \times 3.5 \times 7\ mm^3$ with the compression axis, corresponding to the larger dimension, perpendicular to the interface planes. A total strain of -0.5 was performed on all the samples at a strain rate of $10^{-4}\,s^{-1}$. The

0022–2461 © *1997 Chapman & Hall*

time needed to reach the testing temperature was approximately one hour and a homogenization period of 40 min was systematically applied before testing.

The crystallographic texture was measured in the compression samples by a simplified X-ray procedure [6, 11, 12], where the I_{hkl} reflections obtained from the X-ray diffraction on a sample face are normalized with regard to a non-textured sample according to [12]:

$$p(h\,k\,l) = \frac{I_{hkl}/I^{s}_{hkl}}{(1/N_{peaks})\sum_{hkl}(I_{hkl}/I^{s}_{hkl})} \quad (1)$$

where the superscript s refers to a standard non-textured sample (database JCPDS no. 10-173). The number of peaks having the highest intensities considered here (N_{peaks}) is 10. Due to the $p(h\,k\,l)$ parameter, this semi-quantitative method identifies the tendency for a $(h\,k\,l)$ plane to be parallel to the irradiated sample surface. The (1 0 10) peak was chosen, instead of the (0 0 1) peak which is the main slip plane activated during plastic deformation of alumina [6], because of its larger X-ray intensity and since the corresponding plane makes a small angle (17.5°) with the basal plane (0 0 1).

3. Experimental results

3.1. Microstructural characterization of the sintered materials

Table I summarizes the constitutive parameters (mean grain size, $\langle d \rangle$, shape parameter, *Sh*, % theoretical density, ρ) of the materials in the as-received conditions. The materials possess similar and ultrafine grain sizes. This is unusual since a reduction of the mean grain size of the composite is generally obtained when zirconia particles are added to an alumina matrix [13]. Significant differences in density are found depending on the zirconia content in the composites. The microstructures can be considered as equiaxed since the values of *Sh* are close to unity. A typical as-received microstructure is shown in Fig. 1 for AZ20. The dark grains correspond to the zirconia grains located in intergranular positions. Most of the zirconia grains are twinned as a result of the martensitic transformation from the tetragonal to the monoclinic structure which is expected to occur during cooling after sintering. From TEM observations, it was concluded that the grains were nearly dislocation free. As for the other composites, the sizes of the alumina and zirconia grains are similar. Some cavities

TABLE I Microstructural parameters of the as-received materials

Microstructural parameters	Materials			
	AZ0 (0 vol % ZrO_2)	AZ5 (5 vol % ZrO_2)	AZ10 (10 vol % ZrO_2)	AZ20 (20 vol % ZrO_2)
$\langle d \rangle$ (μm)	0.21	0.20	0.21	0.20
Sh (±0.05)	1.06	1.03	1.04	1.04
ρ (% $\rho_{Theo.}$)	91	90	94	95

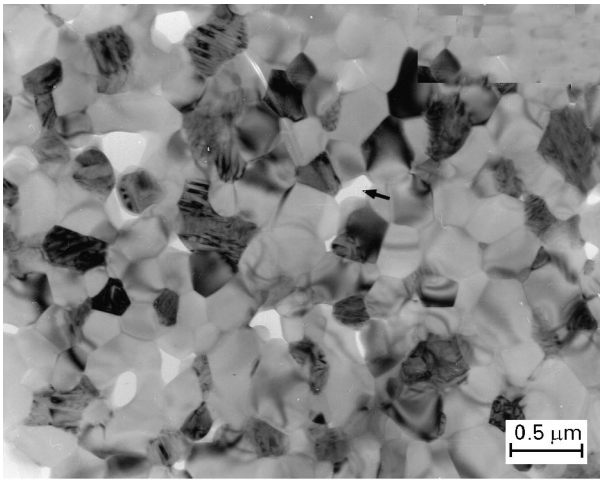

Figure 1 TEM micrograph of AZ20 in the as-received condition.

can be detected, but only those which are surrounded by rounded grains can be attributed to the residual porosity (arrow in Fig. 1); the others are the result of foil preparation. No intragranular cavities are observed in any of the samples.

3.2. Mechanical behaviour

The high-temperature superplastic deformation in ceramics is usually discussed on the basis of the following power law creep relationship:

$$\dot{\varepsilon} = A \exp\left(\frac{-Q_{app}}{RT}\right)\frac{\sigma^{n}}{d^{p}} \quad (2)$$

where $\dot{\varepsilon}$ is the strain rate, σ is the flow stress, d is the grain size, n and p are the stress and grain size exponents, respectively, Q_{app} is the apparent activation energy, A is a constant, and R is the gas constant and T is absolute temperature. From previous data [14], it has been demonstrated that n does not depend significantly on the zirconia content and is close to 2 in the experimental domain of deformation ($1300\,^{\circ}C \leqslant T \leqslant 1400\,^{\circ}C$ and $\dot{\varepsilon} = 10^{-4}\,s^{-1}$). Apparent activation energies were also estimated and found to be $Q_{app} \approx 650 \pm 50\,kJ\,mol^{-1}$ for the composites and $Q_{app} \approx 500 \pm 50\,kJ\,mol^{-1}$ for pure alumina. These results are in relatively good agreement with previously reported data of superplastic deformation of alumina–zirconia composites [2, 15] and pure alumina [6, 12], which indicates that the residual porosity does not seem to influence significantly the values of Q_{app}. Therefore, it was concluded that the deformation of the materials is performed under superplastic conditions.

Fig. 2 shows the influence of temperature on the stress–strain curves in the case of the AZ20 composite. A nearly steady-state regime is rapidly reached in the first stages of the deformation as soon as the compressive strain is greater than 0.05. A similar behaviour was obtained in the case of the AZ10 composite [14], but, when the deformation is performed on the materials with a lower relative density in the as-received conditions (AZ0 and AZ5), the steady-state regime is achieved at a larger strain. This is illustrated by Fig. 3,

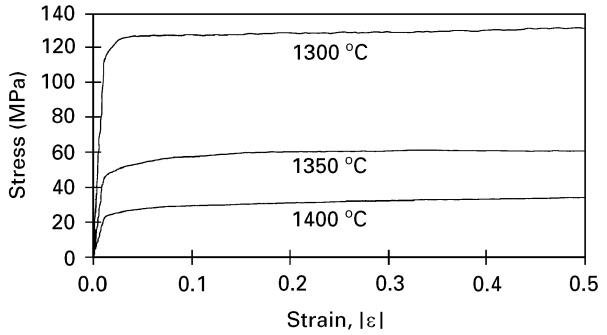

Figure 2 Stress–strain curves of AZ20 at $\dot{\varepsilon} = 10^{-4}\,s^{-1}$.

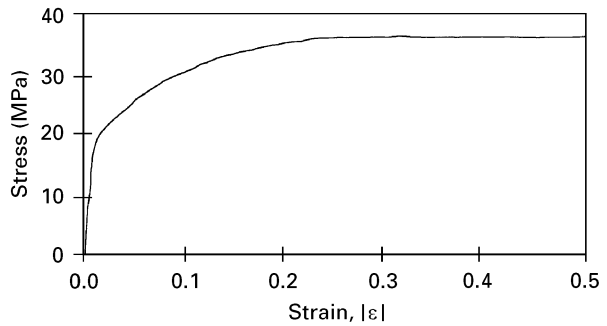

Figure 3 Stress–strain curve of AZ5 at 1400 °C and $\dot{\varepsilon} = 10^{-4}\,s^{-1}$.

which shows the stress–strain curve of AZ5 at $T = 1400\,°C$. In order to get data concerning the variation of density during compression tests, interrupted tests ($\varepsilon = -0.1,\ -0.2,\ -0.3,\ -0.4,\ -0.5$) were systematically performed to estimate the densification rate [14]. It was shown that the strain hardening which occurs during the first stages of the deformation results mainly from strain-induced densification.

3.3. Deformed materials

TEM micrographs of AZ20 and AZ5 deformed at 1400 °C ($\dot{\varepsilon} = 10^{-4}\,s^{-1}$, $\varepsilon = -0.5$) are shown in Figs 4 and 5. The size and the location of the zirconia particles are not significantly affected by deformation (Fig. 4). As illustrated in Fig. 6, grain growth takes place during deformation and is reduced by increasing the zirconia content. The mean grain size remains smaller than 1 μm whatever the experimental conditions and the compositions of the materials. The maximum value of the mean grain size after deformation was obtained in pure alumina deformed at 1400 °C ($\langle d \rangle = 0.60$ μm). TEM micrographs of the deformed samples (Figs 4 and 5) indicate that the microstructures are still fairly equiaxed which confirms the superplastic character of the deformation.

The variations of density induced by deformation are shown in Fig. 7. Densification systematically occurs during compression for all materials and at all temperatures. It must be noted that the densities after deformation appear to be relatively independent of the testing temperature. If AZ10 and AZ20 can be considered as dense (>98%) after compression, AZ0 and AZ5 still retain some porosity after deformation.

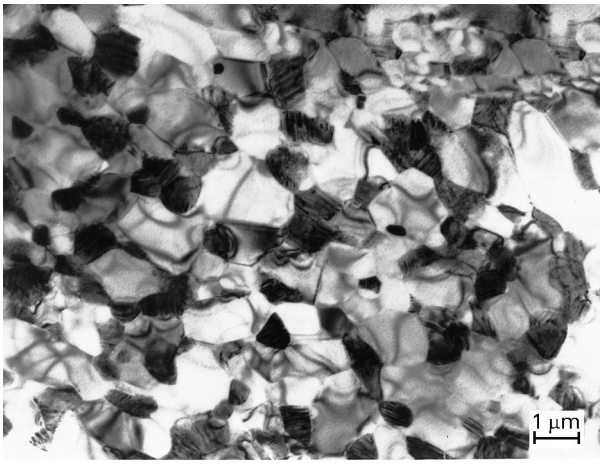

Figure 4 TEM micrograph of AZ20 deformed at 1400 °C.

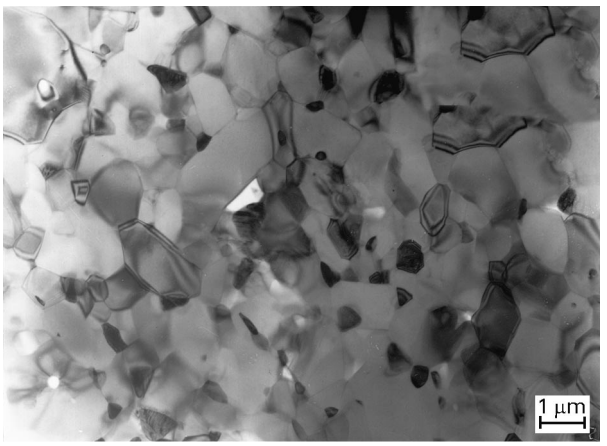

Figure 5 TEM micrograph of AZ5 deformed at 1400 °C.

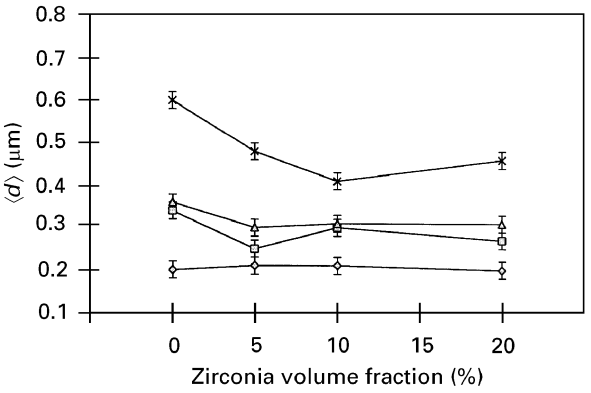

Figure 6 Grain size variation with the deformation temperature. Key: —◇— as received; —□— 1300 °C; —△— 1350 °C; —×— 1400 °C.

4. Discussion

4.1. Method for the evaluation of the GBS contribution

Generally, the GBS contribution can be estimated by measurement, using scanning electron microscopy (SEM), of the offsets in marker lines at grain boundaries [8, 9]. However, this technique cannot be used in the case of ultrafine grained ceramics for which the observation of the microstructure can only be performed by transmission electron microscopy. The

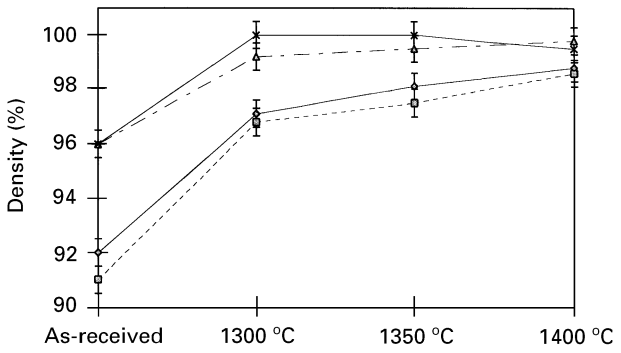

Figure 7 Density variations during deformation. Key: —◇— AZ0; – – –□– – – AZ5; – – –△– – – AZ10; – – –×– – – AZ20.

evaluation of strain due to the GBS (ε_{GBS}) can be carried out by an indirect technique as previously reported by Wakai and Kato [16], Martinez *et al.* [17] and Gruffel [12]. These authors assume that the total strain ε_T is the sum of two contributions: ε_{GBS} and ε_G, where ε_G is the strain due to intragranular deformation. In the case of the materials investigated in this study, this expression must be modified to account for sample densification during compression. The macroscopic strain can be consequently expressed as:

$$\varepsilon_T = \varepsilon_{GBS} + \varepsilon_G + \varepsilon_D \quad (3)$$

where ε_D is the strain due to densification along the compression axis [18].

ε_D depends on the experimental conditions that lead to densification. When the material is freely sintered (no applied stress) and under the assumption of isotropic densification and of a homogenous material, ε_D can be expressed as:

$$\varepsilon_D = \frac{1}{3}\varepsilon_V = \frac{1}{3}\ln\frac{\rho_0}{\rho} \quad (4)$$

where ε_V is the volumic strain, ρ_0 the initial density and ρ the final density.

If sintering is performed by hot pressing in a simple die, the strain in the direction perpendicular to the axis of the applied load is equal to zero ($\varepsilon_x = \varepsilon_y = 0$). The deformation due to densification is therefore produced along the axis of the applied load ($\varepsilon_D = \varepsilon_z = \varepsilon_V$) and ε_D is related to the variation of density according to:

$$\varepsilon_D = \ln\frac{\rho_0}{\rho} \quad (5)$$

In the case of uniaxial compression of porous materials, no analytical relation between ε_D and ρ has been clearly established, despite some experimental work dealing with sinter forging of alumina powders [19]. Consequently, only conditions corresponding to unconstrained sintering and hot pressing in a simple die can be considered. ε_D can thus be estimated according to:

$$\frac{1}{3}\ln\frac{\rho_0}{\rho} < \varepsilon_D < \ln\frac{\rho_0}{\rho} \quad (6)$$

However, even if the upper bound is considered, the contribution of ε_D to the total strain is small ($\varepsilon_D/\varepsilon_T < 0.1$), based on the experimental variations of ρ obtained in this study (Fig. 7) the strain due to intragranular deformation can be deduced from measurement of the elongation of the grains according to [12]:

$$\varepsilon_G = \frac{2}{3}\ln\frac{Sh_I}{Sh_F} \quad (7)$$

where the subscripts I and F refer to the initial and final states, respectively.

It must be underlined, however, that this relation is based on two hypotheses, namely, the equiaxiality of the initial microstructure and the isotropy of grain growth. If one of these hypotheses is not satisfied, Relation 7 may lead to an overestimation of the contribution of the intragranular deformation. The calculation of *Sh* before deformation may be quite delicate to interpret since a random spatial distribution of elongated grains may result in a value of *Sh* close to unity. Moreover in the case of alumina based materials, it has been demonstrated that grain growth is not isotropic [20] and can be enhanced along particular crystallographic orientations [10].

4.2. Variations of the shape parameter

Previously reported data based on this technique (Relation 7) have demonstrated the major contribution of GBS, since values of ε_{GBS} ranging from 60 to 80% of the total strain were found for alumina and alumina–zirconia composites in the superplastic regime [12, 16, 17]. The shape parameters (*Sh*) measured after the compressive tests are reported in Table II. The relative contributions of the intragranular deformation (ε_G) calculated from Equation 7 is summarized in Table III for the three temperatures investigated. The precision of ε_G is obtained from the derivation of Equation 7 and it is found that this precision is within $\pm$ 10%. In spite of the scatter in the results, these

TABLE II Values of *Sh* ($\pm$0.05) at different deformation temperatures

Deformation temperature	Materials			
	AZ0	AZ5	AZ10	AZ20
1300 °C	1.13	1.16	1.12	1.26
1350 °C	1.18	1.15	1.26	1.17
1400 °C	1.17	1.29	1.20	1.23

TABLE III Contribution of the intragranular deformation (%) from Equation 7

Deformation temperature	Materials			
	AZ0	AZ5	AZ10	AZ20
1300 °C	10	15	10	25
1350 °C	15	15	25	15
1400 °C	15	30	20	20

values, which are an upper bound of the intragranular strain, confirm the major contribution of GBS for these materials in the experimental domain investigated. From Table III, it can be concluded that no significant differences are observed between the various materials.

Thus, it is interesting to use another way to determine ε_G. This can be done qualitatively via the measurement of the basal texture of alumina before and after deformation, since intragranular deformation is generally associated with the development of a texture [12, 21].

4.3. Texture variations

Fig. 8 shows the variation with zirconia content of $p(1\,0\,10)$ for planes parallel and perpendicular to the loading direction. Since values of $p(1\,0\,10)$ are systematically close to unity, it can be concluded that no basal texture is developed during the uniaxial sintering. Figs 9, 10, 11 show the variation with zirconia content of $p(1\,0\,10)$ after deformation for planes which are parallel and perpendicular to the compression axis. The influence of the deformation temperature is small, except perhaps for AZ5 at 1400 °C. However,

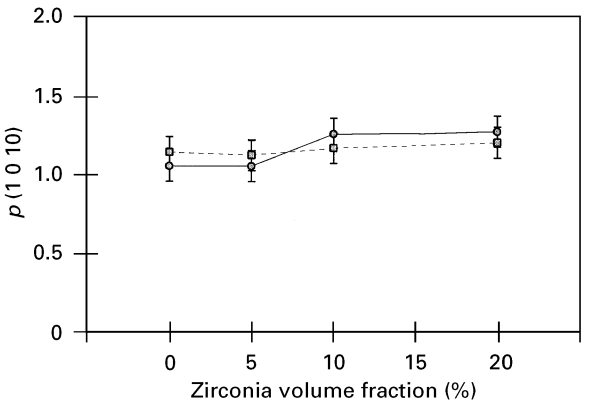

Figure 8 Evolution of p (1 0 10) with the zirconia content and according to the position of the planes with reference to the axial stress of sintering. As-received materials. Key: —◎— perpendicular; – – –▨– – – parallel.

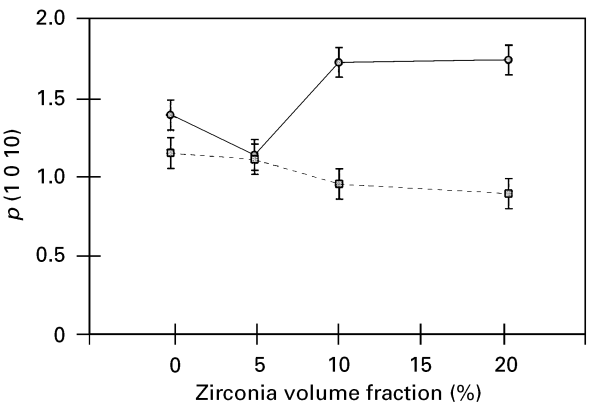

Figure 9 Evolution of p (1 0 10) with the zirconia content and according to the position of the planes with reference to the axial stress of compression. Materials deformed at 1300 °C. Key: —◎— perpendicular; – – –▨– – – parallel.

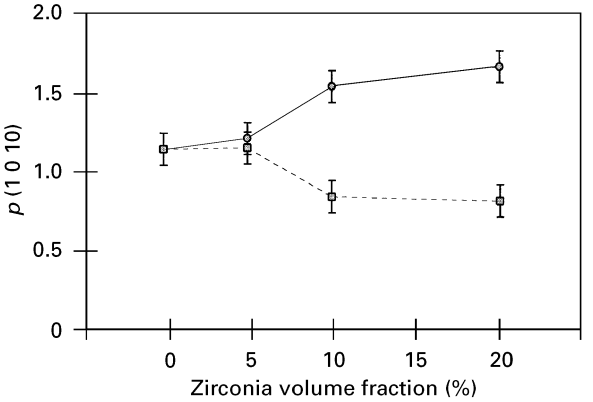

Figure 10 Evolution of p (1 0 10) with the zirconia content and according to the position of the planes with reference to the axial stress of compression. Materials deformed at 1350 °C. Key: —◎— perpendicular; – – –▨– – – parallel.

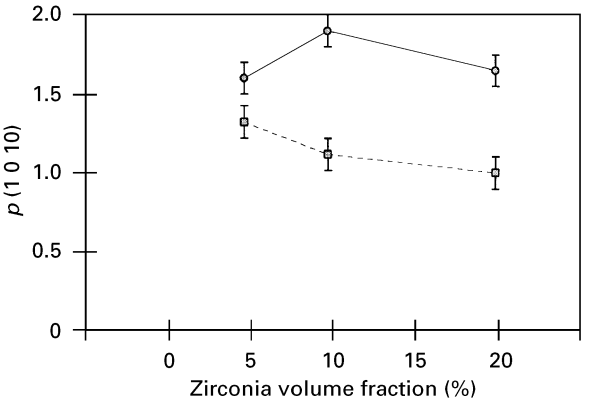

Figure 11 Evolution of p (1 0 10) with the zirconia content and according to the position of the planes with reference to the axial stress of compression. Materials deformed at 1400 °C. Key: —◎— perpendicular; – – –▨– – – parallel.

different behaviours were obtained depending on the zirconia content. AZ0 and AZ5 do not develop a significant texture, whereas in the case of AZ10 and AZ20, $p(1\,0\,10)$ is greater than 1.5 in the planes perpendicular to the deformation axis and lower than 1 in the planes parallel to the deformation axis. This means that a basal texture is induced by deformation, namely that the c-axis of the alumina grains tends to be parallel to the direction of the applied stress. All these results are in good agreement with previous work dealing with the development of texture during superplastic deformation of dense alumina by Fridez [11] and Gruffel [12]. In particular, these authors observed that at 1450 °C and with similar stress levels, values of $p(1\,0\,10)$ close to two were consistent with a predominantly intergranular deformation mode.

These results lead to the conclusion that some differences, in the contribution of plastic deformation to the total strain by a dislocation activity, exist between the materials which exhibit significant residual porosity before deformation (AZ0 and AZ5) and the materials which are nearly dense in the as-received conditions (AZ10 and AZ20). It should be noted that this difference was not revealed by the estimation of the Sh variations. Consequently, it can be inferred that

the hypotheses required for the calculation of ε_G, according to Relation 7, are possibly not fulfilled. In particular, it can be hypothesized that the as-received microstructures were not perfectly equiaxed but that the grains are elongated in random directions. In this case, *Sh* would be equal to unity but would be unacceptable to describe the equiaxiality of the microstructure.

4.4. The GBS contribution

Based on the experimental results: (i) the contribution of the densification strain to total displacement is systematically very limited ($<10\%$), (ii) the initial microstructures are similar and (iii) the contribution of plastic deformation is larger for the materials which exhibit the lower residual porosity in the as-received condition; it can be concluded that the residual porosity affects the GBS contribution during superplastic deformation. Indeed, grain boundary sliding generates stress concentrations at triple junctions [22], which can be released by plastic deformation in the adjacent grains [6]. In the case of materials with significant residual porosity before deformation, stress concentrations are expected to be reduced. Such behaviours were particularly observed at 1300, 1350 and to a lesser extent at 1400 °C, since a noticeable densification takes place at this temperature for AZ5 (Fig. 7). Besides, superplastic deformation of porous ceramics has already been demonstrated, both in compression [23, 24] and tensile conditions [25].

Finally, the GBS contribution to the total strain can be estimated to be greater than 90% for AZ0 and AZ5 ($\varepsilon_D < 10\%$, $\varepsilon_G \approx 0$) and greater than 70% for AZ10 and AZ20 ($\varepsilon_D < 10\%$, $\varepsilon_G < 20\%$). These values can be compared to previously reported data on superplastic deformation of structural ceramics, obtained from measurements of the grain shape change (Relation 7) [12, 16, 17] or of the offsets in marker lines across grain boundaries [7, 8, 18], which led in both cases to values of GBS contributions between 70 and 80% of the macroscopic strain. The particularly high value obtained for AZ0 and AZ5 can be attributed to the residual porosity which allows GBS accommodation and reduces the contribution of intragranular deformation.

5. Conclusions

Superplastic deformation of alumina–zirconia composites has been demonstrated. The contribution of intragranular deformation was estimated from both texture formation and variation of the grain shape. Differences are observed between these two methods and care must be taken in the use of the parameter *Sh* to quantify the grain shape change, since it may be unsuitable to describe some particular grain morphologies. The materials with the greater residual porosity ($\approx 10\%$) had a higher GBS contribution ($>90\%$) to superplastic strain than the more densified materials (GBS $> 70\%$). Consequently, the achievement of ultrafine microstructures with well distributed, ultrafine and intergranular residual porosity after sintering, could permit some shape flexibility by superplastic forming.

Acknowledgements

The authors are grateful to Dr K. P. Plucknett, Dr C. H. Caceres and Professor D. S. Wilkinson from McMaster University (Hamilton, Canada) for having prepared the materials.

References

1. M. F. ASHBY and R. A. VERRALL, *Acta Metall.* **21** (1973) 149.
2. I. W. CHEN and L. A. XUE, *J. Amer. Ceram. Soc.* **73** (1990) 2585.
3. J. D. FRIDEZ, C. CARRY and A. MOCELLIN, "*Advances in Ceramics*", Vol. **10**, edited by N. Claussen, M. Rühle and A. Heuer (The American Ceramic Society, 1985) pp. 720–740.
4. T. CHANDRA, J. J. JONAS and D. M. R. TAPLIN, *J. Mater. Sci.* **13** (1978) 2380.
5. R. Z. VALIEV, O. A. KAIBYSHEV, V. V. ASTANIN and A. K. EMALETDINOV, *Phys. Status Solidi* (*a*) **78** (1983) 439.
6. R. M. CANNON, W. H. RHODES and A. H. HEUER, *J. Amer. Ceram. Soc.* **63** (1980) 46.
7. W. R. CANNON and O. D. SHERBY, *ibid.* **60** (1977) 44.
8. A. H. CHOKSHI, *J. Mater. Sci.* **25** (1990) 3221.
9. T. G. LANGDON, *J. Amer. Ceram. Soc.* **58** (1975) 92.
10. S. LARTIGUE KORINEK and F. DUPAU, *Acta Metall.* **42** (1994) 293.
11. J. D. FRIDEZ, PhD thesis, no. 656, Lausanne, E.P.F.L. (1986).
12. P. GRUFFEL, PhD thesis, no. 921, Lausanne, E.P.F.L. (1991).
13. K. OKADA, Y. YOSHIZAWA and T. SAKUMA, *J. Amer. Ceram. Soc.* **74** (1991) 2820.
14. O. FLACHER, J. J. BLANDIN and K. P. PLUCKNETT, *Mater. Sci. Eng. A* (1997).
15. K. OKADA, Y. YOSHIZAWA and T. SAKUMA, in "Superplasticity in Advanced Materials", edited by S. Hori, M. Tokizane and N. Furushiro (1991) pp. 227–232.
16. R. WAKAI and H. KATO, *Adv. Ceram. Mater.* **3** (1988) 71.
17. R. MARTINEZ, R. DUCLOS and J. CRAMPON, *Scripta Metall. Mater.* **24** (1990) 1979.
18. T. HERMANSSON, K. P. D. LAGERLÖF and G. L. DUNLOP, in Proceedings of Superplasticity and Superplastic Forming, edited by C. H. Hamilton and N. E. Paton (TMS, 1988) pp. 631–635.
19. K. R. VENKATACHARI and R. RAJ, *J. Amer. Ceram. Soc.* **69** (1986) 499.
20. J. RÖDEL and A. M. GLAESER, *ibid.* **73** (1990) 3292.
21. O. A. KAIBYSHEV, I. V. KAZACHKOV and I. V. ALEXANDROV, *Acta Metall.* **32** (1984) 585.
22. A. BALL and M. M. HUTCHINSON, *Met. Sci. J.* **3** (1969) 1.
23. T. E. CHUNG and T. J. DAVIES, *Acta Metall.* **27** (1979) 627.
24. I. A. AKMOULIN, M. DJAHAZI and J. J. JONAS, *Scripta Metall. Mater.* **25** (1991) 1035.
25. Z. C. WANG, T. J. DAVIES and N. RIDLEY, *ibid.* **30** (1994) 355.

Received 25 March
and accepted 23 October 1996